

Learning Modality-Aware Representations: Adaptive Group-wise Interaction Network for Multimodal MRI Synthesis

Tao Song, Yicheng Wu, Minhao Hu, Xiangde Luo, Linda Wei, Guotai Wang, Yi Guo, Feng Xu, Shaoting Zhang

Abstract— Multimodal MR image synthesis aims to generate missing modality images by effectively fusing and mapping from a subset of available MRI modalities. Most existing methods adopt an image-to-image translation paradigm, treating multiple modalities as input channels. However, these approaches often yield sub-optimal results due to the inherent difficulty in achieving precise feature- or semantic-level alignment across modalities. To address these challenges, we propose an Adaptive Group-wise Interaction Network (AGI-Net) that explicitly models both inter-modality and intra-modality relationships for multimodal MR image synthesis. Specifically, feature channels are first partitioned into predefined groups, after which an adaptive rolling mechanism is applied to conventional convolutional kernels to better capture feature and semantic correspondences between different modalities. In parallel, a cross-group attention module is introduced to enable effective feature fusion across groups, thereby enhancing the network’s representational capacity. We validate the proposed AGI-Net on the publicly available IXI and BraTS2023 datasets. Experimental results demonstrate that AGI-Net achieves state-of-the-art performance in multimodal MR image synthesis tasks, confirming the effectiveness of its modality-aware interaction design. We release the relevant code at: <https://github.com/zunzhumu/Adaptive-Group-wise-Interaction-Network-for-Multimodal-MRI-Synthesis.git>.

Index Terms— MR Image Synthesis; Group-wise Interaction; Adaptive Rolling; Cross-group Attention

I. INTRODUCTION

Tao Song is with the School of Information Science and Technology, Fudan university, Shanghai 200438, China, and also Shanghai AI Lab, Shanghai 200232, China (email:tsong22@m.fudan.edu.cn).

Yicheng Wu is with the Faculty of Information Technology, Monash University, Melbourne, VIC 3800, Australia.

Minhao Hu is with the Wellcome Centre for Integrative Neuroimaging, Nuffield Department of Clinical Neurosciences, University of Oxford, Oxford, OX3 9DU, UK.

Xiangde Luo and Guotai Wang are with the School of Mechanical and Electrical Engineering, University of Electronic Science and Technology of China, Chengdu 611731, China.

Linda Wei is with the Department of Computer Science and Engineering, The Chinese University of Hong Kong, Hong Kong.

Yi Guo and Feng Xu are with the School of Information Science and Technology, Fudan university, Shanghai 200438, China.

Shaoting Zhang is with Shanghai AI Lab, Shanghai 200232, China, and also with SenseTime Research, Shanghai 200233, China (email:Zhangshaoting@pjlab.org.cn).

ULTIMODA medical data plays an important role in modern clinical diagnosis and treatment by providing diverse, complementary information about organs and tissues, aiming at enhancing both accuracy and confidence in clinical decision-making. For example, the MRI T1 modality is usually used to indicate human anatomies and the T2 modality can highlight soft tissues. However, factors such as patient non-compliance during scanning, extended scanning times, and the degradation of individual modality hinder the broader adoption of multimodal imaging [1], [2]. As a result, it is highly desirable to synthesize missing modalities from a limited number of available multimodal data [3]–[6].

Similar to image translation tasks, multimodal medical image synthesis typically necessitates modeling the interrelationships between modalities, integrating fine-grained cross-modal features, and learning mappings from multiple input modalities to a single target modality. By leveraging complementary information across modalities, multimodal synthesis generally reduces the complexity of network learning and improves the reliability of the generated outputs compared to natural image-to-image translation. However, in clinical practice, even after registration, multiple MRI modalities often exhibit imperfect alignment in terms of both features and semantic structures. This challenge is further exacerbated in multi-acquisition multimodal datasets, where no absolute ground truth exists for fully aligned cross-modal representations.

In recent years, significant progress has been made in the field of multimodal MR image synthesis. Approaches such as learning modality-specific representations and latent representations of multimodal images [7]–[10] have been extensively studied. Fusion strategies like Multi-Scale Gate Mergence [11], attention-based fusion [12], and Confidence-Guided Aggregation [13] further have been explored. These methods typically involve multiple networks or branches for fine-grained intra-modality feature extraction and use shared fusion networks to capture inter-modality relationships, significantly increasing the training and inference costs of the models. Moreover, they do not address the issue of feature and semantic misalignment in the feature fusion process between different modalities. However, designing a single effective network capable of performing fine-grained intra-modality feature extraction while capturing inter-modality relationships under feature and semantic misaligned conditions remains an

unresolved challenge.

It is widely recognized that the quality of features extracted by neural networks is crucial for medical image synthesis. Deep models are required to extract fine-grained features from different modalities and capture local feature and semantic interactions. Since multimodal images are almost impossible to align perfectly in feature and semantic locations (e.g., different tissue structures in T1 or T2 modality), most traditional convolution designs are challenging to achieve optimal performance.

Therefore, in this paper, we study the task of multimodal MR image synthesis and propose a simple yet effective Adaptive Group-wise Interaction Network (AGI-Net), with the key design of Cross Group Attention and Group-wise Rolling (CAGR) module. Here, Cross Group Attention establishes intra-group and inter-group relationships to suppress inter-modality aliasing noise in the input features, while Group-wise Rolling allows independent adaptive rolling of convolution kernels across groups to adjust the kernel positions for each group (as illustrated in Fig. 1), with the rolling offsets predicted by a *routing function* in a data-dependent manner. These two group-based designs work seamlessly together, effectively capturing inter-modality local feature and semantic relationships under partial misalignment, thus enhancing the network to extract and integrate information across different modalities. The proposed module is a plug-and-play component that can replace any convolution layer. We evaluate our approach on the publicly available IXI¹ and BraTS2023² datasets, and extensive experiments conducted by replacing the convolution module within existing frameworks demonstrate the effectiveness of our AGI-Net, achieving a new state of the art for multimodal MR image synthesis.

II. RELATED WORK

A. Multimodal Image Synthesis.

Multimodal image synthesis improves upon traditional single-modality image synthesis by extracting intra-modality features and capturing inter-modality correlations, thereby enhancing synthesis accuracy and reliability. Numerous studies have focused on designing various adversarial networks to better capture detailed anatomical structures. For instance, [14] explores adversarial networks for detailed structure capture, while [14]–[16] proposes conditional adversarial networks to enhance the synthesis of multi-contrast MR images. [17] employs progressively grown generative adversarial networks for high-resolution medical image synthesis, and [18] utilizes unified multimodal generative adversarial networks for multimodal MR image synthesis. Similarly, [19] introduces a collaborative generative adversarial network for missing image synthesis.

Another research direction involves developing more adaptive multimodal fusion networks based on extracting modality-specific features with dedicated modality networks. For example, [7] uses a hierarchical mixed fusion block to learn correlations between multimodal features, enabling adaptive weighted fusion of features from different modalities. [11]

employs a multi-scale gate mergence mechanism to automatically learn weights of different modalities, enhancing relevant information while suppressing irrelevant information. [13] proposes a confidence-guided aggregation module that adaptively aggregates target images in multimodal image synthesis based on corresponding confidence maps. [12] uses a mixed attention fusion module to integrate high-level semantic information and low-level fine-grained features across different layers, adaptively exploiting rich, complementary representative information.

Although the aforementioned approaches have proven effective, they generally focus on constructing various types of adversarial networks and multi-network fusion networks, with limited exploration of the feature extraction challenges posed by imperfect alignment between different modalities.

B. Dynamic Convolution.

Standard convolution maintains constant parameters and locations throughout the entire inference process, whereas dynamic convolution allows for flexible adjustments to both parameters and locations based on different inputs, offering advantages in computational efficiency and representational power. Dynamic convolution can typically be classified into two categories: 1) adaptive kernel shape and 2) adaptive kernel parameters. Adaptive kernel shape involves generating suitable kernel shapes according to different inputs. For instance, [20]–[23] generates kernel deformations through offsets to capture more accurate semantic information, while [24] constrains the kernel shape into a snake-like form to capture vascular continuity features.

Adaptive kernel parameters, on the other hand, utilize input-generated kernel weights. For example, [25], [26] proposed adaptive rotating kernels to capture objects in various orientations for rotation-invariant object detection. [27]–[29] adapts kernel parameters by deformation to handle object deformation while maintaining a consistent receptive field. The method proposed in this paper falls under the category of adaptive kernel parameters. The proposed convolution module employs group-wise rolling kernel parameters, which alleviates the issue of imperfect alignment between modalities and enhances the network's ability to represent multimodal images.

III. METHOD

An overview of our core CAGR module is shown in Fig. 4. The CAGR primarily consists of the Cross Group Attention module and Group-wise Rolling module. The function of the Cross Group Attention module is to selectively suppress aliasing noise caused by irrelevant modality features and enhance the expression of relevant modality features by leveraging both intra-group and inter-group information. The Group-wise Rolling module is to dynamically perform group-wise rolling of convolutional kernels based on the predicted offsets. In this section, we begin by introducing the intra-group and inter-group attention mechanisms used in the Cross Group Attention module. Next, we explain the group-wise rolling mechanism for convolutional kernels with specified offsets within the Group-wise Rolling module. Finally, we provide details on the network implementation based on the CAGR module.

¹<https://brain-development.org/ixi-dataset/>

²<https://www.med.upenn.edu/cbica/brats/>

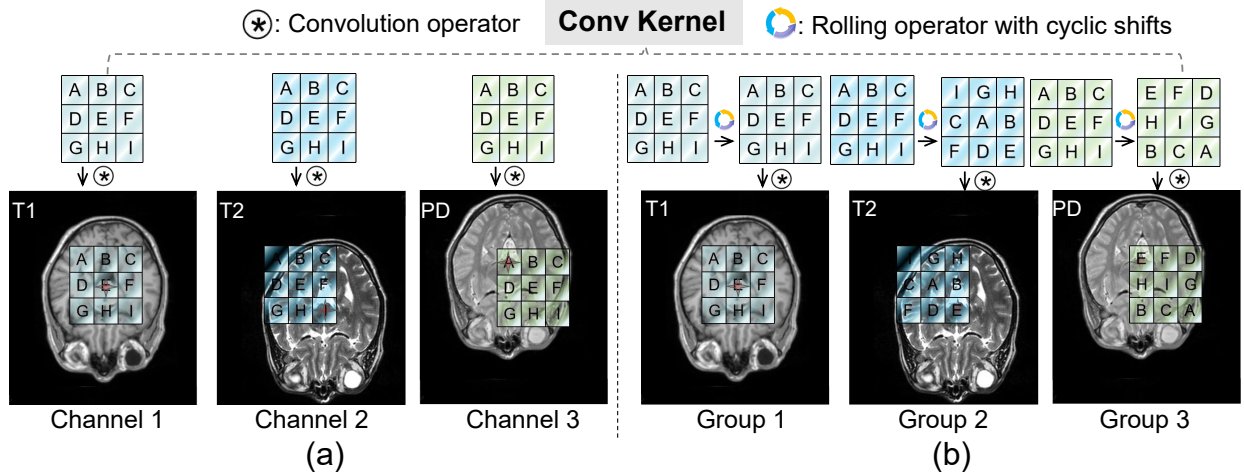


Fig. 1: Comparison between rolling convolution and standard convolution with a 3-channel image input. (a) Illustration of standard convolution, where the locations of parameters in each convolution kernel remain fixed across channels. (b) Illustration of rolling convolution, where the convolution weights shift in a data-dependent manner to capture feature and semantic variations across different groups.

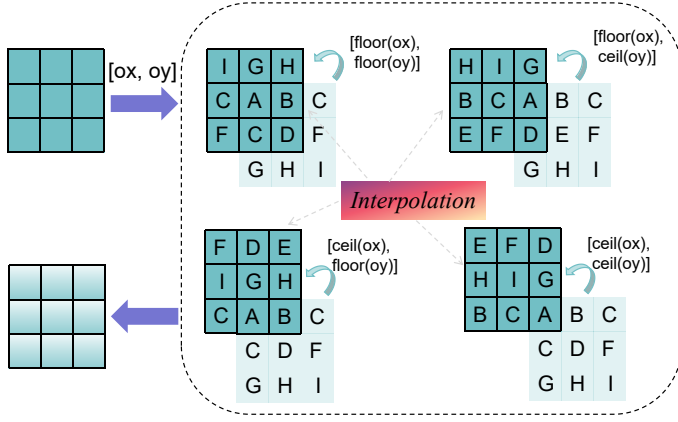


Fig. 2: Illustrating the rolling process of a convolutional kernel with a size of 3. Initially, the floating-point offsets of the kernel along the x-axis and y-axis are predicted. Subsequently, four sets of convolution kernels are generated through integer displacement operations. Finally, interpolation is employed to obtain the kernel weights corresponding to the floating-point displacements.

A. Cross Group Attention

Before performing the rolling convolution operation, for multimodal image synthesis tasks, the input feature $x \in \mathbb{R}^{C_{in} \times H_{in} \times W_{in}}$ can be easily divided into n groups, where each group $x_i, i \in \{1, 2, \dots, n\}$ contains feature information related to a specific modality. However, after multiple layers of convolution, each group x_i may incorporate features from other modalities, leading to aliasing noise, which reduces the accuracy of subsequent rolling offset prediction. To address this issue, we employ a Cross Group Attention mechanism. This mechanism selectively suppresses aliasing noise caused by irrelevant modality features and enhances the expression of relevant modality features by leveraging both intra-group and

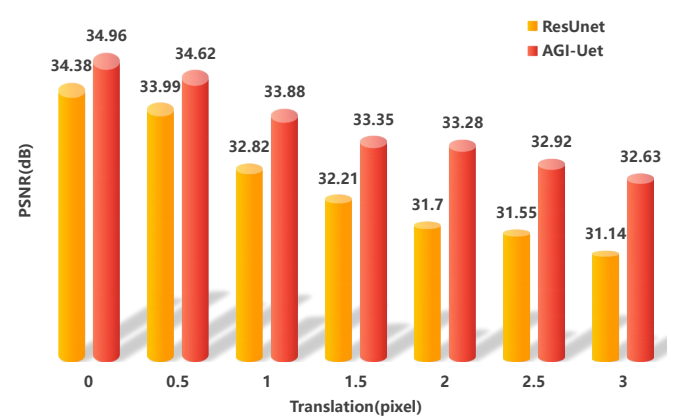


Fig. 3: Random translation perturbation test result with the pixel2pixel framework for the (T1, T2)->PD scenario on the IXI dataset. Random translation perturbation is applied to the pre-registered T2 modality images in the T1 and T2 pair.

inter-group information.

Specifically, we first apply average pooling to each group feature x_i obtaining the intra-group pool feature z_i . Then, using a channel shuffle [30], [31] operation, we rearrange the channels of z to construct inter-group information flow, producing the inter-group feature z_i^s . The concatenation of intra-group and inter-group features is then fed through a convolution layer F followed by a Sigmoid function to generate an attention map.

$$A_i = \sigma(F(concat[z_i, z_i^s])) \quad (1)$$

Finally, the attention map is used to perform element-wise multiplication with the input feature x , resulting in enhanced intra-group features and weakened inter-group interference

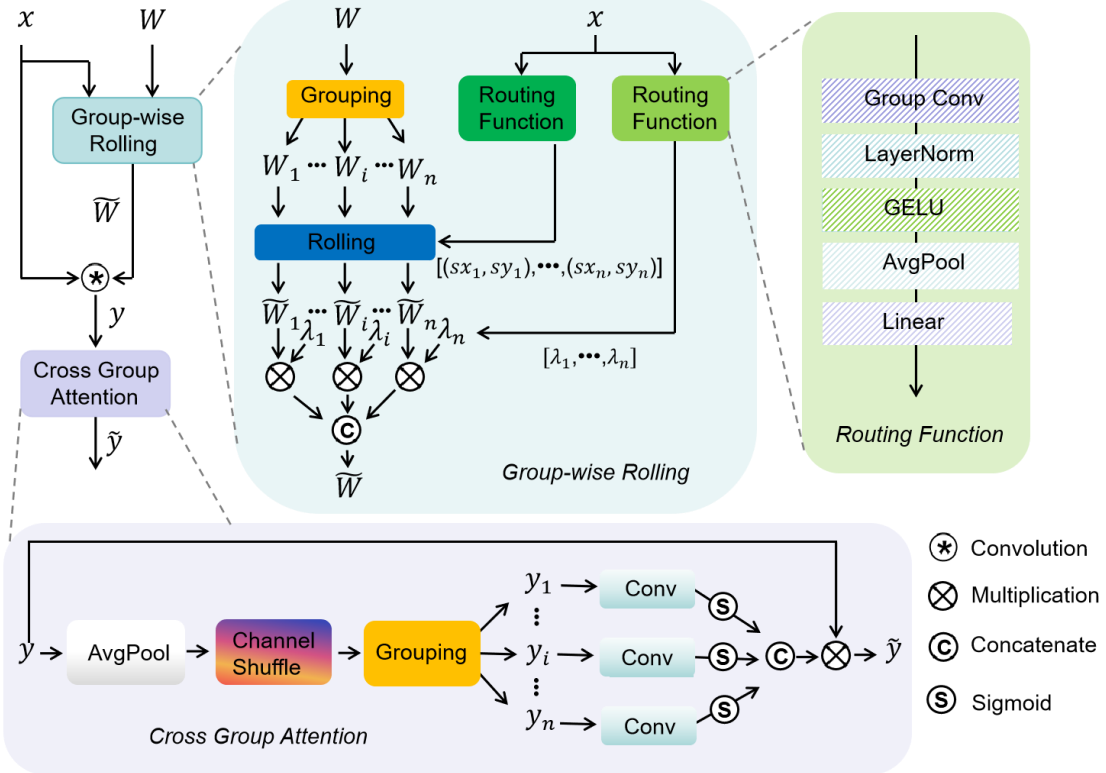


Fig. 4: An overview of our proposed CAGR module, which contains two components: Cross Group Attention and Group-wise Rolling. The Cross Group Attention module enhances the input features prior to the Group-wise Rolling module to reduce noise. Following this, the Group-wise Rolling module rolls the convolution kernels in a group-wise manner using the offsets learned from the enhanced input features.

features. The modified feature \tilde{x} is then used as the input for the subsequent group-wise rolling convolution.

$$\tilde{x} = \{x_i \odot A_i\}, i \in \{1, 2, \dots, n\} \quad (2)$$

B. Group-wise Rolling

In this section, we provide a detailed explanation of the Group-wise Rolling module within CAGR. This module operates in two main steps: predicting the parameters for rolling convolution based on the enhanced input features by Cross Group Attention, and generating group-wise rolled convolution kernels.

To predict the rolling offsets for each group in a data-dependent manner, we designed a lightweight network called the *routing function*. The *routing function* takes the enhanced input image feature \tilde{x} as input and predicts n groups rolling offsets $[(ox_1, oy_1), \dots, (ox_n, oy_n)]$ for kernels. Each group independently predicts offsets $\{ox_i\}_{i \in \{1, 2, \dots, n\}}$ and $\{oy_i\}_{i \in \{1, 2, \dots, n\}}$ along the x-axis and y-axis, respectively. The overall architecture of the *routing function* is illustrated in Fig. 4. Initially, the enhanced input image feature $\tilde{x} \in \mathbb{R}^{C_{in} \times H_{in} \times W_{in}}$ is fed into a lightweight Group convolution [32] with a kernel size of 3×3 , followed by Layer Normalization [33], [34]

and GELU [35] activation. The activated features are then average pooled to form a feature vector of dimension C_{in} . This pooled feature vector is passed into two separate branches. The first branch is the rolling offset prediction branch, which predicts offsets along the x-axis and y-axis for each group. No activation function is applied to the predicted offsets, enhancing the expressive power of the rolling convolution. The second branch termed the group scale factor prediction branch, is responsible for predicting the scale factor λ for each group. It consists of a linear layer with bias and Sigmoid activation. The weights of both the rolling offset prediction and group scale factor prediction branches in the *routing function* are initialized to zero, and the bias in the group scale factor prediction branch is initialized to one, ensuring stability at the beginning of the training process. Notably, the number of groups n is significantly smaller than the number of input channels of the convolution C_{in} . Consequently, it is straightforward to partition the convolution kernels into n distinct groups across the C_{in} channels, with each group having a unique set of offsets.

The standard convolution takes enhanced input features $\tilde{x} \in \mathbb{R}^{C_{in} \times H_{in} \times W_{in}}$ and kernel weights $W \in \mathbb{R}^{C_{out} \times C_{in} \times k \times k}$, producing the output feature $y \in \mathbb{R}^{C_{out} \times H_{out} \times W_{out}}$. For

the multi-channel enhanced input feature \tilde{x} in multimodal imaging, convolution is applied uniformly across feature and semantic positions with the same kernel weights $\mathbf{w}_m \in \mathbb{R}^{C_{\text{in}} \times k \times k}$, $m \in \{1, 2, \dots, C_{\text{out}}\}$ performing C_{out} operations to obtain the output feature y with C_{out} channels. In our approach, we divide the kernel weights W into n groups $\mathbf{w}_i \in \mathbb{R}^{C_{\text{out}} \times C_{\text{in}}/n \times k \times k}$, $i \in \{1, 2, \dots, n\}$ in C_{in} dimension, where kernels from different groups can independently capture features specific to different modalities through the grouping strategy.

$$\begin{aligned} \mathbf{W} &= \{\mathbf{w}_m \in \mathbb{R}^{C_{\text{in}} \times k \times k}\}, m \in \{1, 2, \dots, C_{\text{out}}\} \\ &= \{\mathbf{w}_i \in \mathbb{R}^{C_{\text{out}} \times C_{\text{in}}/n \times k \times k}\}, i \in \{1, 2, \dots, n\}. \end{aligned} \quad (3)$$

After predicting the rolling offsets and grouping the kernels along the C_{in} dimension, each kernel within the i -th group undergoes rolling based on its corresponding offset, resulting in the rolled kernel group. Additionally, each group of kernels is scaled by a learnable scale factor λ_i , which represents the relative importance of different groups. The final transformation can be expressed by the following equation:

$$\begin{aligned} \tilde{\mathbf{W}} &= \{\lambda_i \times \text{FloatRoll}(\mathbf{w}_i, (ox_i, oy_i))\} \\ &= \{\lambda_i \times a_i \times \text{roll}(\mathbf{w}_i, (f(ox_i), f(oy_i))) \\ &\quad + b_i \times \text{roll}(\mathbf{w}_i, (c(ox_i), f(oy_i))) \\ &\quad + c_i \times \text{roll}(\mathbf{w}_i, (f(ox_i), c(oy_i))) \\ &\quad + d_i \times \text{roll}(\mathbf{w}_i, (c(ox_i), c(oy_i))))\}, i \in \{1, 2, \dots, n\} \end{aligned} \quad (4)$$

where $a_i = (1 - cx_i) \times (1 - cy_i)$, $b_i = cx_i \times (1 - cy_i)$, $c_i = (1 - cx_i) \times cy_i$, $d_i = cx_i \times cy_i$. Here $f(\cdot)$ and $c(\cdot)$ represents *floor* and *ceil* function, respectively. Where $cx_i = ox_i - f(ox_i)$ and $fracy_i = oy_i - f(oy_i)$, respectively. The *roll* denotes an operator based on CUDA that supports batch rolling operations on tensors, whereas the built-in roll function in PyTorch does not support batch rolling.

The detailed process of group-wise rolling for convolution kernels is shown in Fig. 2 and Equation 4. First, the floating-point offsets along the x-axis and y-axis are predicted for each group kernel $\hat{\mathbf{w}}_i$. Then, integer displacement operations are applied to generate four sets of convolution kernels. Finally, interpolation is used to compute the group kernel weights $\tilde{\mathbf{w}}_i$ corresponding to the floating-point offsets. So the $\tilde{\mathbf{W}}$ can be concatenated in the C_{in} dimension by all group-rolled kernel weights. Notably, the number of kernel parameters in Group-wise Rolling convolution is the same as that in standard convolution, rather than being reduced to $1/n$ of the standard convolution parameters as in Group convolution.

C. Network Architecture

In terms of network implementation, since our proposed CAGR module can be easily integrated as a plug-and-play component into any network structure with convolutional layers, we built the proposed network architecture, AGI-Net, based on the commonly used ResUnet [36]. ResUnet consists of three down-sampling stages, three up-sampling stages, and a central body stage. Each stage includes two ResBlocks ($z + F(\text{relu}(F(z)))$). We replaced the first convolution in each ResBlock within the three down-sampling stages, the

body stage, and the first up-sampling stage with the CAGR module to form the new network architecture, referred to as AGI-Net. Ablation studies on replacing different parts of the network and their impact on performance are discussed in the experimental section.

IV. EXPERIMENT

A. Experiment Settings

1) *Datasets*.: We evaluated the proposed method on two publicly available MRI multimodal benchmark datasets: IXI³ and BraTS2023⁴ [37]. From the IXI dataset, we selected 577 patients who had T1, T2, and PD-weighted images. The dataset was randomly split into training, validation, and test sets. The training set comprised 500 patients with a total of 44,935 2D images, the validation set contained 37 patients with 3,330 2D images, and the test set had 40 patients with 3,600 2D images. All images were resized to 256x256. Similarly, from the BraTS2023 dataset, we randomly selected T1, T2, and FLAIR images from 580 patients. This dataset was split into 500 patients for the training set, 40 patients for the validation set, and 40 patients for the test set. In terms of 2D images, the training set contained 40,000 images, the validation set 3,200 images, and the test set 3,200 images, with an image size of 240x240. All MRI modalities were normalized to the [0, 1] range using min-max normalization based on the 99.5th percentile maximum value and a minimum value of 0.

2) *Implementation Details*.: For training, we set the total number of iterations to 120k using the Adam optimizer with a learning rate of 1e-4 and a batch size of 16. All experiments were conducted in a uniform environment using 4 NVIDIA Tesla V100 GPUs. We utilized the widely recognized Peak Signal-to-Noise Ratio (PSNR), Structural Similarity Index (SSIM), and Mean Absolute Error (MAE) metrics to evaluate the image synthesis quality. Although adversarial methods are no longer considered novel, they remain the core algorithm in the BraSyn 2023 Challenge [?], [42] and continue to demonstrate strong performance advantages in multimodal MR image synthesis tasks. Meanwhile, we have also explored more recent diffusion-based approaches.

B. Comparison with state-of-the-art methods

We conducted multimodal image synthesis experiments under three scenarios on both the IXI and BraTS2023 datasets, comparing our method against existing approaches using three metrics: PSNR, SSIM, and MAE. The existing methods are categorized into two types based on their generative framework: 1) Diffusion-based methods, which employ multi-step iterative diffusion and sampling, such as DDPM [38], IDDPMP [39] and SelfRDB [40]; and 2) Adversarial-based methods, which utilize a single-step approach grounded in the adversarial game between a generator and a discriminator, such as pGAN [15], mmGAN [16], MedSynth [14], and pixel2pixel [41]. The *Ours* method integrates AGI-Net with

³<https://brain-development.org/ixi-dataset/>

⁴<https://www.med.upenn.edu/cbica/brats/>

TABLE I: Comparison of experimental results on the IXI dataset with existing methods. The evaluation focuses on multimodal image synthesis across three scenarios: (T2, PD)->T1, (T1, PD)->T2, and (T1, T2)->PD. The *Ours* method integrates AGI-Net with pixel2pixel. Notably, the MAE results are scaled by a factor of 100.

Scenario	(T2, PD)->T1			(T1, PD)->T2			(T1, T2)->PD		
Method	PSNR(dB)	SSIM(%)	MAE	PSNR(dB)	SSIM(%)	MAE	PSNR(dB)	SSIM(%)	MAE
DDPM [38]	26.55	91.26	2.20	28.88	92.02	1.89	32.24	94.77	1.35
IDDPM [39]	26.06	90.24	2.44	28.71	90.28	1.95	32.47	94.35	1.28
selfRDB [40]	28.28	93.07	1.82	31.08	94.35	1.49	34.46	95.45	1.06
mmGAN [16]	28.32	92.98	1.80	30.55	92.74	1.58	33.71	95.04	1.12
pGAN [15]	28.69	93.86	1.73	30.62	92.05	1.63	33.74	95.33	1.10
MedSynth [14]	28.65	93.28	1.73	31.18	94.22	1.45	34.25	95.94	1.03
pixel2pixel [41]	28.77	93.96	1.70	31.20	94.14	1.44	34.38	96.34	1.01
AGI-Net(Ours)	29.23	94.38	1.59	31.71	94.33	1.37	34.96	96.62	0.97

the highly competitive pixel2pixel [41]. As shown in Table. I, Table. II and Table. III, our approach consistently outperforms the existing methods across all multimodal image synthesis scenarios. As shown in Table VIII, replacing the backbone network from ResUnet to AGI-Net leads to significant performance improvements across various adversarial-based methods. However, in diffusion-based frameworks, where each step predicts noise rather than the image itself, AGI-Net encounters difficulty in capturing structural transformations, which consequently results in a performance drop.

C. Ablation Study

We first conducted ablation studies on different components of the CAGR module and compared it with existing dynamic convolution modules by replacing CAGR with these alternatives. The results demonstrate that CAGR not only significantly outperforms standard convolution methods but also surpasses existing dynamic convolution modules. We further analyzed the impact of the number of groups n and the effects of replacing CAGR at different stages of the network. Lastly, we introduced random translations to the input multimodal images to increase misalignment between modalities, verifying the effectiveness of our method.

1) *Cross Group Attention and Group-wise Rolling*.: We compared the performance of the proposed CAGR module with standard convolution on the IXI dataset. As shown in Table. V, we observed that the multimodal image synthesis performance improved through Group-wise Rolling, resulting in a 0.47 dB increase in PSNR on the pixel2pixel [41] framework. The performance was further enhanced with the inclusion of Cross Group Attention. The experimental results demonstrate that the proposed CAGR module effectively captures richer feature and semantic correspondences and facilitates cross-modal feature fusion across different modalities.

2) *Different Dynamic Convolutions*.: We further compared the performance of the proposed CAGR module with existing dynamic convolution methods on the IXI dataset. These dynamic convolutions can be categorized into two types: one based on adaptive kernel shapes, such as Deformable Convolution [22], and the other based on adaptive kernel parameters, such as Adaptive Rotated Convolution (ARC) [25]. Following the same replacement strategy as AGI-Net, we constructed Deform-ResUnet and ARC-ResUnet. As shown in Table. VI,

we found that AGI-Net achieved the greatest improvement in multimodal image synthesis performance, with a PSNR increase of 1.49 dB. The experimental results demonstrate that the proposed CAGR module offers significant advantages over previous dynamic convolution methods in the multimodal image synthesis task.

3) *Number of groups*.: An ablation study was conducted to evaluate the impact of different group numbers within the CAGR module. Intuitively, for the 2-to-1 multimodal image synthesis task, setting $n = 2$ is sufficient to capture the feature and semantic relationships between different modalities. As shown in Table. VII, although $n = 2$ offers a significant performance improvement over standard convolution, the results indicate that as the number of groups increases from 2 to 8, both parameter count and FLOPs decrease while performance improves. However, with $n = 16$, performance begins to degrade, suggesting that $n = 2$ is insufficient to fully capture the misalignment and interrelationships in the multi-channel feature space. Notably, while increasing the number of groups moderately reduces parameters and FLOPs, the best performance ($n = 8$) shows only a slight increase compared to standard convolution. This is because n primarily affects the parameters and FLOPs of the *routing function* and Cross Group Attention’s group convolution, with the Cross Group Attention contributing only a small portion to the overall network.

4) *Random translation perturbations test*.: We further evaluated the performance variation of the proposed CAGR module under increasing feature and semantic misalignment between input multimodal images. Specifically, we introduced random translation perturbations to one of the two default-registered modalities. The perturbation range was divided into seven difficulty levels, from 0 to 3 pixels, with increments of 0.5 pixels. As shown in Fig. 3, although the performance of both AGI-Net and ResUnet decreases as the magnitude of the translation perturbations increases, AGI-Net exhibits a more gradual decline compared to ResUnet. This indicates that the advantage of the proposed AGI-Net becomes more obvious as the misalignment range increases. This further demonstrates that the proposed AGI-Net exhibits inherently superior capabilities in automatic feature and semantic alignment compared to ResUnet, thereby mitigating the significant performance degradation in multimodal MRI synthesis caused

TABLE II: Comparison of experimental results on the BraTS2023 dataset with existing methods. The evaluation focuses on multimodal image synthesis across three scenarios: (T2, FLAIR)->T1, (T1, FLAIR)->T2, and (T1, T2)->FLAIR. The *Ours* method integrates AGI-Net with pixel2pixel. Notably, the MAE results are scaled by a factor of 100.

Scenario	(T2, FLAIR)->T1			(T1, FLAIR)->T2			(T1, T2)->FLAIR		
Method	PSNR(dB)	SSIM(%)	MAE	PSNR(dB)	SSIM(%)	MAE	PSNR(dB)	SSIM(%)	MAE
DDPM [38]	23.72	87.35	2.79	23.14	88.37	2.50	20.14	84.97	4.18
IDDPM [39]	23.78	88.45	2.71	22.40	87.98	2.98	21.91	83.11	3.22
selfRDB [40]	25.41	91.55	2.16	24.65	90.89	2.05	24.04	89.87	2.30
mmGAN [16]	24.92	90.68	2.28	24.21	90.64	2.21	23.39	88.14	2.54
pGAN [15]	25.51	90.89	2.17	24.79	91.31	2.16	23.28	88.08	2.64
MedSynth [14]	25.70	91.11	2.10	24.84	90.98	2.13	24.00	89.06	2.40
pixel2pixel [41]	25.67	91.68	2.10	24.82	91.62	2.13	24.06	89.18	2.37
AGI-Net(Ours)	26.07	92.20	1.98	25.37	92.17	1.95	24.54	89.80	2.22

TABLE III: Comparison of experimental results on the BraTS2023 dataset with existing methods. The evaluation focuses on multimodal image synthesis across three scenarios: (T2, FLAIR, T1Gd)->T1, (T1, FLAIR, T1Gd)->T2, (T1, T2, T1Gd)->FLAIR, and (T1, T2, FLAIR)->T1Gd. The *Ours* method integrates AGI-Net with pixel2pixel. Notably, the MAE results are scaled by a factor of 100.

Scenario	(T2, Flair, T1Gd)->T1			(T1, Flair, T1Gd)->T2		
Method	PSNR(dB)	SSIM(%)	MAE	PSNR(dB)	SSIM(%)	MAE
DDPM [38]	25.36	91.34	2.23	23.60	90.27	2.45
IDDPM [39]	26.08	90.02	2.07	23.50	86.17	2.59
selfRDB [40]	28.20	93.14	1.56	24.06	92.15	2.38
mmGAN [16]	27.26	92.05	1.70	24.77	91.08	2.08
pGAN [15]	27.76	92.36	1.64	25.49	92.24	1.95
MedSynth [14]	28.08	91.69	1.60	25.68	92.59	1.94
pixel2pixel [41]	28.17	93.08	1.57	25.77	92.58	1.92
AGI-Net(Ours)	28.57	93.61	1.51	26.05	92.80	1.85
Scenario	(T1, T2, T1Gd)->Flair			(T1, T2, Flair)->T1Gd		
Method	PSNR(dB)	SSIM(%)	MAE	PSNR(dB)	SSIM(%)	MAE
DDPM [38]	21.80	72.84	3.53	21.99	86.35	3.41
IDDPM [39]	20.93	83.44	3.83	23.83	85.13	2.48±0.69
selfRDB [40]	24.43	89.80	2.31	25.95	90.34	1.86
mmGAN [16]	23.22	87.60	2.58	24.25	88.09	2.25
pGAN [15]	24.08	89.39	2.36	25.68	89.32	1.99
MedSynth [14]	24.42	89.07	2.30	26.01	89.58	1.88
pixel2pixel [41]	24.50	89.93	2.26	26.10	90.39	1.85
AGI-Net(Ours)	24.88	90.43	2.14	26.48	90.78	1.75

TABLE IV: Comparison of brain tumor segmentation results on the BraTS2023 dataset with (T1, T2, Flair)->T1Gd scenarios.

Method	2D Dice(%)	3D Dice(%)
Zeros(lower bound)	44.16	10.59
MedSynth [14]	71.95	51.93
pixel2pixel [41]	72.16	51.12
AGI-Net(Ours)	72.86	53.37
Full modalities(upper bound)	86.31	80.45

TABLE V: Ablation studies on the influence of Group-wise Rolling (GR) and Cross Group Attention (CA) module. The experiments were conducted on the IXI dataset in the (T1, T2)->PD scenario, based on the pixel2pixel framework.

GR	CA	PSNR(dB)	SSIM(%)
-	-	34.38	96.34
✓	-	34.85 (↑0.47)	96.49 (↑0.15)
✓	✓	34.96 (↑0.58)	96.62 (↑0.28)

TABLE VI: Ablation studies on the impact of different convolution types. The experiments were conducted on the IXI dataset using the (T1, T2)->PD modality synthesis task with a 3-pixel translation, based on the pixel2pixel framework.

Method	PSNR(dB)
ResUnet [36]	31.14
Deform-ResUnet [22]	32.09 (↑0.95)
ARC-ResUnet [25]	32.16 (↑1.02)
AGI-Net	32.63 (↑1.49)

TABLE VII: An ablation study on the number of groups n conducted in the (T1, T2)->PD scenario of the IXI dataset.

Network	n	Params(M)	FLOPs(G)	PSNR(dB)	SSIM(%)
ResUnet	-	17.04	141.91	34.38	96.34
AGI-Net	1	33.58	238.84	34.76	96.49
AGI-Net	2	25.31	190.52	34.85	96.55
AGI-Net	4	21.19	166.36	34.93	96.60
AGI-Net	8	19.15	154.28	34.96	96.62
AGI-Net	16	18.18	148.24	34.88	96.60

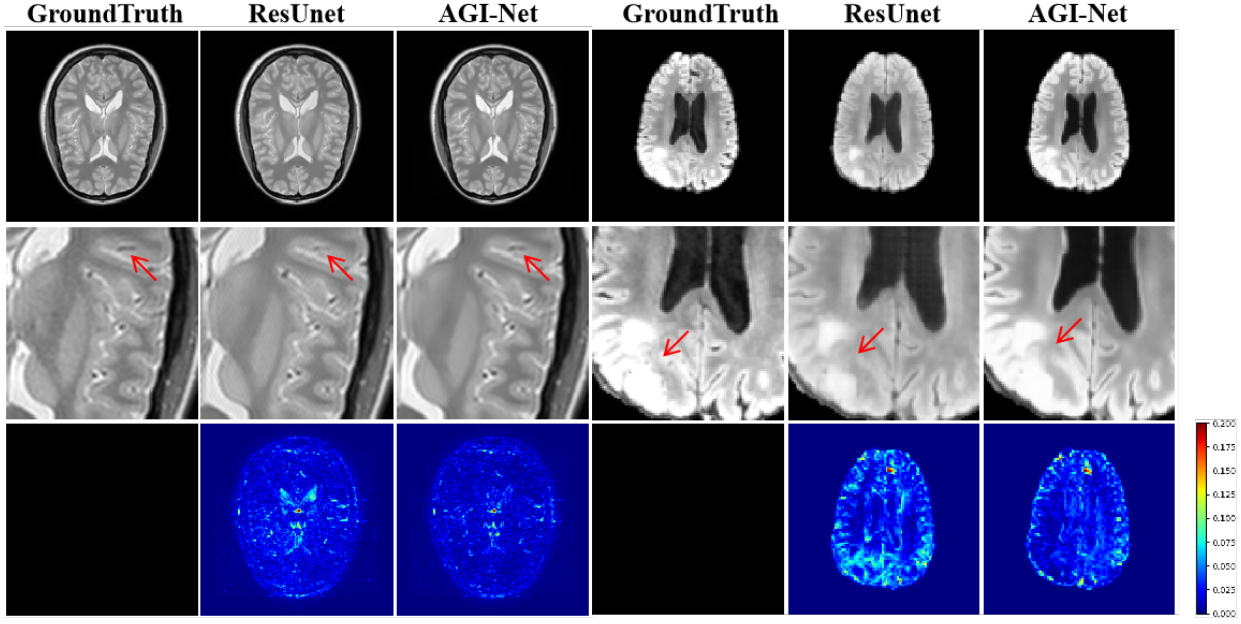


Fig. 5: Displays the (T1, T2)->PD synthesis results of pixel2pixel using the IXI dataset. The first row presents the ground truth along with the synthesis results from ResUnet and AGI-Net. The second row shows an enlarged view of the region of interest (ROI), while the third row illustrates the synthesis error map.

TABLE VIII: Experimental results of network replacement in different methods for the (T1, T2)->PD scenario on the IXI dataset.

Method	Network	PSNR(dB)	SSIM(%)
IDDPMP [39]	ResUnet	32.47	94.35
	AGI-Net	32.15	94.03
selfRDB [40]	ResUnet	34.46	95.45
	AGI-Net	34.05	95.01
mmGAN [16]	ResUnet	33.71	95.04
	AGI-Net	34.10	95.46
pGAN [15]	ResUnet	33.74	95.33
	AGI-Net	34.33	95.59
pixel2pixel [41]	ResUnet	34.38	96.34
	AGI-Net	34.96	96.62

by registration-induced uncertainty and errors in real clinical scenarios.

5) Replacement strategy.: We conducted experiments to replace the convolutional layers in all stages of ResUnet with the proposed CAGR module. As shown in Table 2, as the number of replaced stages increases, there is a gradual improvement in terms of parameters, FLOPs, and PSNR compared to the baseline model, reaching peak performance when all five initial stages are replaced. Therefore, we selected the configuration with the first five stages replaced to construct our AGI-Net.

6) Brain Tumor Segmentation.: We perform brain tumor segmentation using a UNet model trained on real BraTS 2023 MRI data. Both 2D and 3D Dice scores are reported in Table IV under (T1, T2, FLAIR) → T1Gd scenarios. Our key findings are as follows: (1) Zero-imputation of missing

modalities leads to a significant performance drop, highlighting the importance of proper modality handling. (2) AGI-Net, which leverages synthesized modalities, outperforms both MedSynth [14] and pixel2pixel [41] by a substantial margin in segmentation accuracy. (3) Despite being trained in a 2D setting, AGI-Net exhibits strong 3D consistency in brain tumor segmentation on the BraTS 2023 dataset, demonstrating its robustness in volumetric analysis.

7) Exploration of 3D Image Synthesis.: We extend existing 2D synthesis methods to 3D and train them on the BraTS 2023 MRI dataset. As shown in Table X, we report the performance of mmGAN [16], pGAN [15], MedSynth [14], and pixel2pixel [41] in comparison with our proposed method. The results demonstrate that even when AGI-Net is extended to a 3D architecture, our approach continues to exhibit strong performance.

8) Visualization.: To better illustrate the synthesis performance of our method, we visualize the error maps and regions of interest (ROIs). The experiments were conducted on the IXI test set using a pixel-to-pixel framework. As demonstrated in Fig. 5, the synthesis results of AGI-Net show greater structural consistency with the ground truth compared to ResUnet, proving the superior adaptability of our method in capturing and fusing misaligned features across multiple modalities. Fig. 6 presents a comparative analysis of PCA feature maps across different feature stages of ResUnet and AGI-Net. The results clearly indicate that AGI-Net demonstrates superior noise resilience and captures more detailed structural information.

D. Limitation and Future Work

Although the proposed AGI-Net demonstrates superior performance in multimodal MR image synthesis, addressing po-

TABLE IX: An ablation study on the strategy of replacing standard convolutions in the network architecture for the (T1, T2)->PD scenario of the IXI dataset.

Down1	Down2	Down3	Body	Up1	Up2	Up3	Params(M)	FLOPs(G)	PSNR(dB)
-	-	-	-	-	-	-	17.04	141.91	34.38
✓	-	-	-	-	-	-	17.06	144.46	34.62
✓	✓	-	-	-	-	-	17.12	146.95	34.73
✓	✓	✓	-	-	-	-	17.47	149.40	34.80
✓	✓	✓	✓	-	-	-	18.81	151.83	34.93
✓	✓	✓	✓	✓	-	-	19.15	154.28	34.96
✓	✓	✓	✓	✓	✓	-	19.24	156.76	34.93
✓	✓	✓	✓	✓	✓	✓	19.26	159.31	34.92

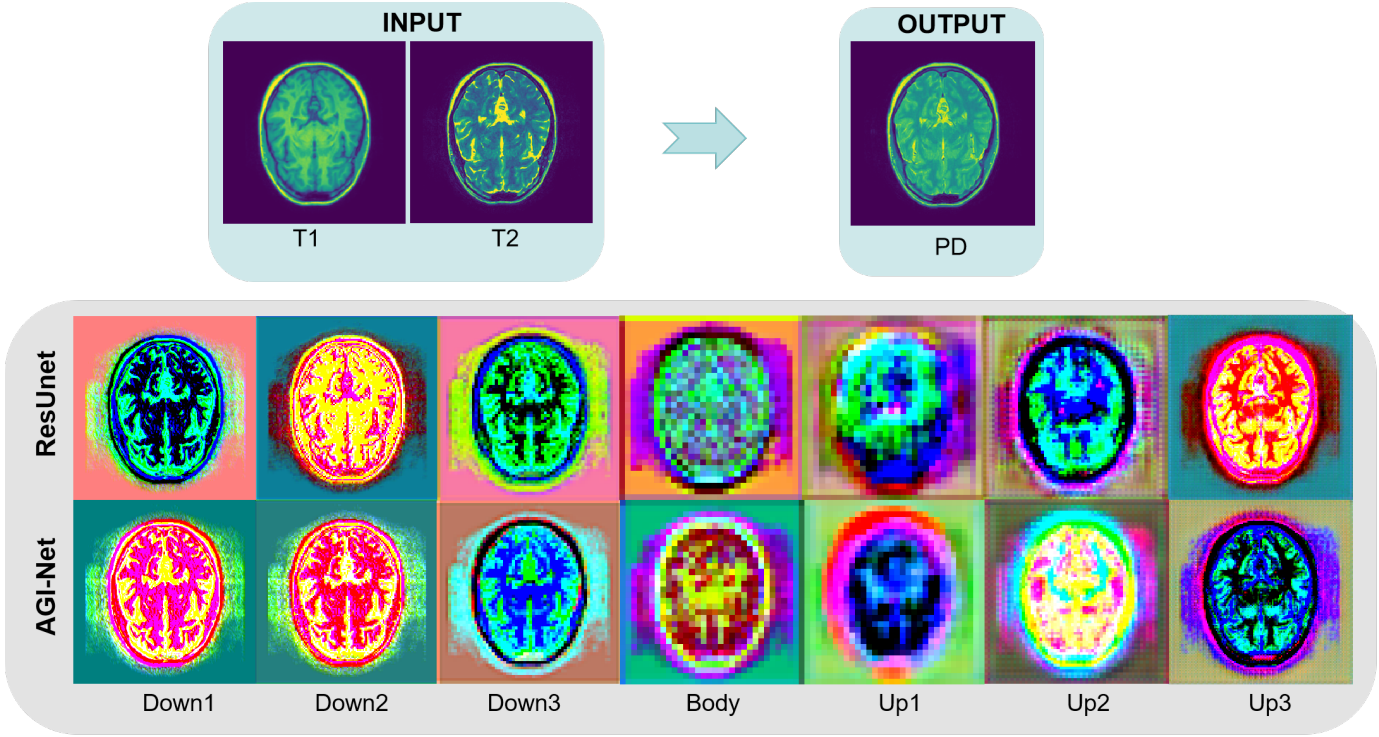


Fig. 6: We visualized the features of ResUnet and AGI-Net, color-coded using principal component analysis (PCA).

TABLE X: Comparison of Experimental Results on the BraTS2023 Dataset with Existing 3D Methods. The evaluation targets multimodal MRI synthesis for the task (T1, T2, FLAIR) → T1Gd. Our proposed method (*Ours*) integrates a 3D AGI-Net with a 3D pix2pix framework. Note that the reported MAE values are scaled by a factor of 100 for clarity.

Method	PSNR(dB)	SSIM(%)	MAE
3D mmGAN [16]	23.76	88.08	2.52
3D pGAN [15]	24.94	89.31	2.26
3D MedSynth [14]	25.30	89.53	2.12
3D pixel2pixel [41]	25.37	89.66	2.01
3D AGI-Net(<i>Ours</i>)	25.84	90.00	1.90

tential feature and semantic misalignments between the input multimodal images and the target modality remains challenging. Future work will involve this and focus on developing a unified synthesis framework to further reduce costs in clinical

deployments.

V. CONCLUSIONS

We present an adaptive group-wise interaction model for multimodal MR image synthesis, featuring two key components: the Cross-Group Attention and Group-wise Rolling modules. The Cross-Group Attention module is designed to fuse both intra-group and inter-group information, effectively mitigating feature and semantic misalignment between different modality groups. Following this, the convolutional kernels are adaptively rolled in a data-driven manner based on the specific modality groups. This module is flexible and can be integrated into any convolutional backbone for multimodal MR image synthesis. Experimental results show that our AGI-Net significantly enhances image synthesis performance on public multimodal benchmarks while maintaining computational efficiency.

REFERENCES

- [1] B. B. Thukral, "Problems and preferences in pediatric imaging," *Indian Journal of Radiology and Imaging*, vol. 25, no. 04, pp. 359–364, 2015.
- [2] K. Krupa and M. Bekiesińska-Figatowska, "Artifacts in magnetic resonance imaging," *Polish journal of radiology*, vol. 80, p. 93, 2015.
- [3] J. E. Iglesias, E. Konukoglu, D. Zikic, B. Glocker, K. Van Leemput, and B. Fischl, "Is synthesizing mri contrast useful for inter-modality analysis?" in *Medical Image Computing and Computer-Assisted Intervention-MICCAI 2013: 16th International Conference, Nagoya, Japan, September 22-26, 2013, Proceedings, Part I 16*. Springer, 2013, pp. 631–638.
- [4] Y. Huo, Z. Xu, S. Bao, A. Assad, R. G. Abramson, and B. A. Landman, "Adversarial synthesis learning enables segmentation without target modality ground truth," in *2018 IEEE 15th international symposium on biomedical imaging*. IEEE, 2018, pp. 1217–1220.
- [5] Y. Wu, T. Song, Z. Wu, Z. Ge, Z. Chen, and J. Cai, "Codebrain: Impute any brain mri via instance-specific scalar-quantized codes," *arXiv preprint arXiv:2501.18328*, 2025.
- [6] J. Liu, S. Pasumarthi, B. Duffy, E. Gong, K. Datta, and G. Zaharchuk, "One model to synthesize them all: Multi-contrast multi-scale transformer for missing data imputation," *IEEE transactions on medical imaging*, vol. 42, no. 9, pp. 2577–2591, 2023.
- [7] T. Zhou, H. Fu, G. Chen, J. Shen, and L. Shao, "Hi-net: hybrid-fusion network for multi-modal mr image synthesis," *IEEE transactions on medical imaging*, vol. 39, no. 9, pp. 2772–2781, 2020.
- [8] T. Joyce, A. Chartsias, and S. A. Tsaftaris, "Robust multi-modal mr image synthesis," in *Medical Image Computing and Computer Assisted Intervention- MICCAI 2017: 20th International Conference, Quebec City, QC, Canada, September 11-13, 2017, Proceedings, Part III 20*. Springer, 2017, pp. 347–355.
- [9] A. Chartsias, T. Joyce, M. V. Giuffrida, and S. A. Tsaftaris, "Multi-modal mr synthesis via modality-invariant latent representation," *IEEE transactions on medical imaging*, vol. 37, no. 3, pp. 803–814, 2017.
- [10] X. Meng, K. Sun, J. Xu, X. He, and D. Shen, "Multi-modal modality-masked diffusion network for brain mri synthesis with random modality missing," *IEEE Transactions on Medical Imaging*, 2024.
- [11] B. Zhan, D. Li, X. Wu, J. Zhou, and Y. Wang, "Multi-modal mri image synthesis via gan with multi-scale gate mergence," *IEEE Journal of Biomedical and Health Informatics*, vol. 26, no. 1, pp. 17–26, 2021.
- [12] H. Li, Y. Han, J. Chang, and L. Zhou, "Hybrid generative adversarial network based on a mixed attention fusion module for multi-modal mr image synthesis algorithm," *International Journal of Machine Learning and Cybernetics*, vol. 15, no. 6, pp. 2111–2130, 2024.
- [13] B. Peng, B. Liu, Y. Bin, L. Shen, and J. Lei, "Multi-modality mr image synthesis via confidence-guided aggregation and cross-modality refinement," *IEEE Journal of Biomedical and Health Informatics*, vol. 26, no. 1, pp. 27–35, 2021.
- [14] D. Nie, R. Trullo, J. Lian, L. Wang, C. Petitjean, S. Ruan, Q. Wang, and D. Shen, "Medical image synthesis with deep convolutional adversarial networks," *IEEE Transactions on Biomedical Engineering*, vol. 65, no. 12, pp. 2720–2730, 2018.
- [15] S. U. Dar, M. Yurt, L. Karacan, A. Erdem, E. Erdem, and T. Cukur, "Image synthesis in multi-contrast mri with conditional generative adversarial networks," *IEEE transactions on medical imaging*, vol. 38, no. 10, pp. 2375–2388, 2019.
- [16] A. Sharma and G. Hamarneh, "Missing mri pulse sequence synthesis using multi-modal generative adversarial network," *IEEE transactions on medical imaging*, vol. 39, no. 4, pp. 1170–1183, 2019.
- [17] A. Beers, J. Brown, K. Chang, J. P. Campbell, S. Ostmo, M. F. Chiang, and J. Kalpathy-Cramer, "High-resolution medical image synthesis using progressively grown generative adversarial networks," *arXiv preprint arXiv:1805.03144*, 2018.
- [18] H. Li, J. C. Paetzold, A. Sekuboyina, F. Kofler, J. Zhang, J. S. Kirschke, B. Wiestler, and B. Menze, "Diamondgan: unified multi-modal generative adversarial networks for mri sequences synthesis," in *Medical Image Computing and Computer Assisted Intervention-MICCAI 2019: 22nd International Conference, Shenzhen, China, October 13–17, 2019, Proceedings, Part IV 22*. Springer, 2019, pp. 795–803.
- [19] D. Lee, J. Kim, W.-J. Moon, and J. C. Ye, "Collagan: Collaborative gan for missing image data imputation," in *Proceedings of the IEEE/CVF conference on computer vision and pattern recognition*, 2019, pp. 2487–2496.
- [20] J. Dai, H. Qi, Y. Xiong, Y. Li, G. Zhang, H. Hu, and Y. Wei, "Deformable convolutional networks," in *Proceedings of the IEEE international conference on computer vision*, 2017, pp. 764–773.
- [21] X. Zhu, H. Hu, S. Lin, and J. Dai, "Deformable convnets v2: More deformable, better results," in *Proceedings of the IEEE/CVF conference on computer vision and pattern recognition*, 2019, pp. 9308–9316.
- [22] W. Wang, J. Dai, Z. Chen, Z. Huang, Z. Li, X. Zhu, X. Hu, T. Lu, L. Lu, H. Li *et al.*, "Internimage: Exploring large-scale vision foundation models with deformable convolutions," in *Proceedings of the IEEE/CVF conference on computer vision and pattern recognition*, 2023, pp. 14 408–14 419.
- [23] Y. Xiong, Z. Li, Y. Chen, F. Wang, X. Zhu, J. Luo, W. Wang, T. Lu, H. Li, Y. Qiao *et al.*, "Efficient deformable convnets: Rethinking dynamic and sparse operator for vision applications," in *Proceedings of the IEEE/CVF Conference on Computer Vision and Pattern Recognition*, 2024, pp. 5652–5661.
- [24] Y. Qi, Y. He, X. Qi, Y. Zhang, and G. Yang, "Dynamic snake convolution based on topological geometric constraints for tubular structure segmentation," in *Proceedings of the IEEE/CVF International Conference on Computer Vision*, 2023, pp. 6070–6079.
- [25] Y. Pu, Y. Wang, Z. Xia, Y. Han, Y. Wang, W. Gan, Z. Wang, S. Song, and G. Huang, "Adaptive rotated convolution for rotated object detection," in *Proceedings of the IEEE/CVF International Conference on Computer Vision*, 2023, pp. 6589–6600.
- [26] J. Wang, Y. Pu, Y. Han, J. Guo, Y. Wang, X. Li, and G. Huang, "Gra: Detecting oriented objects through group-wise rotating and attention," *arXiv preprint arXiv:2403.11127*, 2024.
- [27] H. Gao, X. Zhu, S. Lin, and J. Dai, "Deformable kernels: Adapting effective receptive fields for object deformation," *arXiv preprint arXiv:1910.02940*, 2019.
- [28] B. Kim, J. Ponce, and B. Ham, "Deformable kernel networks for joint image filtering," *International Journal of Computer Vision*, vol. 129, no. 2, pp. 579–600, 2021.
- [29] Q. Chen, C. Li, J. Ning, S. Lin, and K. He, "Gmconv: Modulating effective receptive fields for convolutional kernels," *IEEE Transactions on Neural Networks and Learning Systems*, 2024.
- [30] X. Zhang, X. Zhou, M. Lin, and J. Sun, "Shufflenet: An extremely efficient convolutional neural network for mobile devices," in *Proceedings of the IEEE conference on computer vision and pattern recognition*, 2018, pp. 6848–6856.
- [31] N. Ma, X. Zhang, H.-T. Zheng, and J. Sun, "Shufflenet v2: Practical guidelines for efficient cnn architecture design," in *Proceedings of the European conference on computer vision (ECCV)*, 2018, pp. 116–131.
- [32] A. Krizhevsky, I. Sutskever, and G. E. Hinton, "Imagenet classification with deep convolutional neural networks," *Advances in neural information processing systems*, vol. 25, 2012.
- [33] T. ValizadehAslani and H. Liang, "Layernorm: A key component in parameter-efficient fine-tuning," *arXiv preprint arXiv:2403.20284*, 2024.
- [34] A. Vaswani, "Attention is all you need," *Advances in Neural Information Processing Systems*, 2017.
- [35] D. Hendrycks and K. Gimpel, "Gaussian error linear units (gelus)," *arXiv preprint arXiv:1606.08415*, 2016.
- [36] K. Zhang, Y. Li, W. Zuo, L. Zhang, L. Van Gool, and R. Timofte, "Plug-and-play image restoration with deep denoiser prior," *IEEE Transactions on Pattern Analysis and Machine Intelligence*, vol. 44, no. 10, pp. 6360–6376, 2021.
- [37] D. LaBella, U. Baid, O. Khanna, S. McBurney-Lin, R. McLean, P. Nedelec, A. Rashid, N. H. Tahon, T. Altes, R. Bhalerao *et al.*, "Analysis of the brats 2023 intracranial meningioma segmentation challenge," *arXiv preprint arXiv:2405.09787*, 2024.
- [38] J. Ho, A. Jain, and P. Abbeel, "Denoising diffusion probabilistic models," in *Advances in Neural Information Processing Systems*, vol. 33, 2020, pp. 6840–6851.
- [39] A. Q. Nichol and P. Dhariwal, "Improved denoising diffusion probabilistic models," in *Proceedings of the International Conference on Machine Learning*, vol. 139, 2021, pp. 8162–8171.
- [40] F. Arslan, B. Kabas, O. Dalmaz, M. Ozbey, and T. Çukur, "Self-consistent recursive diffusion bridge for medical image translation," *arXiv preprint arXiv:2405.06789*, 2024.
- [41] P. Isola, J.-Y. Zhu, T. Zhou, and A. A. Efros, "Image-to-image translation with conditional adversarial networks," in *Proceedings of the IEEE conference on computer vision and pattern recognition*, 2017, pp. 1125–1134.
- [42] H. B. Li, G. M. Conte, Q. Hu, S. M. Anwar, F. Kofler, I. Ezhov, K. van Leemput, M. Piraud, M. Diaz, B. Cole *et al.*, "The brain tumor segmentation (brats) challenge 2023: Brain mr image synthesis for tumor segmentation (bratsyn)," *ArXiv*, pp. arXiv–2305, 2024.